Valence-electron contributions to the electric-field gradient in hcp metals and at Gd nuclei in intermetallic compounds with the $ThCr_2Si_2$ structure

R. Coehoorn and K. H. J. Buschow
Philips Research Laboratories, 5600 JA Eindhoven, The Netherlands

M. W. Dirken and R. C. Thiel
Kamerlingh Onnes Laboratorium, 2300 RA Leiden, The Netherlands

(Received 8 January 1990; revised manuscript received 6 April 1990)

Self-consistent band-structure calculations have been used to calculate valence-electron contributions to the electric-field gradient (EFG) in all elemental hcp metals, except those with nonspherical $4f$ shells, and at Gd nuclei in numerous intermetallic compounds of the type GdT_2Si_2 (T=Cr, Mn, Fe, Co, Ni, Cu, Ru, Rh, Pd, Ag, Os, Ir, and Ag) and $GdNi_2X_2$ (X=Ge and Sn). Experimental determinations of the EFG in the latter two compounds were performed by a study of the ^{155}Gd Mössbauer effect. The calculated EFG of hcp metals agrees well with the experimental values. The variation of the EFG with the T component across a given RT_2Si_2 series (R=rare earth, $T=3d$, $4d$, $5d$) is shown to be mainly due to a change of the asphericity of the Gd $6p$ charge distribution. The trends in this asphericity have also been explained qualitatively from a more simple treatment of the electronic structure, based on Miedema's "macroscopic-atom" model for cohesion in metals. It is shown that as a consequence of the large valence-electron contribution to the EFG, the commonly used proportionality relation between the EFG and the second-order crystal-field parameter A_2^0 lacks a true physical basis, and may be invalid.

I. INTRODUCTION

Measurements of the electric-field gradient (EFG) at Gd nuclei in rare-earth–transition-metal intermetallic compounds, e.g., by Mössbauer spectroscopy, have been used frequently to study the contribution of rare-earth atoms to the magnetocrystalline anisotropy.[1–5] This contribution is due to the interaction between the aspherical electrostatic potential at the rare-earth site and the aspherical charge cloud of the $4f$ electrons. Gd is an excellent probe atom for measurements of the contribution to the EFG from non-$4f$ electrons because its spherically symmetric $4f$ shell does not contribute to the EFG.

In the analysis of the experimental results, in which the EFG V_{zz} at the nucleus is related to the crystal-field parameter A_2^0, one has often used the point-charge model, in which the electrostatic potential at the central atom is calculated from a lattice summation over the contributions of point charges on neighbor sites. A firm physical basis for the use of the point-charge model for metals is missing. It is well known that in metals charges are screened very well. In particular, the use of large ionic charges is highly unrealistic, and additional contributions from the own valence electrons of the rare earths to the EFG cannot be neglected. For the elemental metals, this contribution is expected to be the dominant source of the EFG because charge-transfer effects between dissimilar atoms are absent. Recent first-principles calculations by Blaha, Schwarz, and Dederichs[6] for nonmagnetic hcp metals up to Z=48 (Cd), and for ferromagnetic hcp Co, have confirmed this point.

In this paper we present further evidence of the importance of the asphericity of the valence-electron charge density to the EFG. First, calculations are presented of the EFG in all hcp elemental metals, including the elements above Z=48, except those with nonspherical $4f$ shells. The aspherical valence-electron charge densities were obtained from augmented-spherical-wave (ASW) band-structure calculations. The contributions from p and d valence shells are represented in a physically transparent way, viz., in terms of the occupation numbers of the subshells and $\langle r^{-3} \rangle$ expectation values of the radial wave functions. Within the ASW method, although a spherical approximation for the potential is made, the resulting charge density is nonspherical. Calculations for the hcp metals show that, in spite of this approximation, the resulting values of V_{zz} are quite accurate. The advantage of using the ASW method is its computational efficiency, which will permit calculations for crystal structures with complicated unit cells, for which calculations with full-potential methods are extremely time consuming. Considerable attention has been paid to the origin of the EFG in hcp Gd in view of the above-mentioned interest in the EFG at Gd nuclei in intermetallic compounds.

In the second part of this paper, calculations of the EFG at Gd nuclei in intermetallic compounds of the GdT_2X_2 type, with the $ThCr_2Si_2$ structure ($T=3d$, $4d$, and $5d$ transition-metal atoms, X=Si, Ge, or Sn), are presented. The observed trends in the EFG cannot be explained on the basis of the point-charge model.[4] We will show that V_{zz} is determined to a large extent by the valence-electron contribution. The trends in the asphericity of the valence-electron charge density in these com-

pounds are shown to follow from a simple treatment of the local electronic structure, based on Miedema's "macroscopic-atom" model.

Within the point-charge model, the electric-field gradient at the Gd site is proportional to the second-order crystal-field parameter A_2^0.[2] However, if there is a large contribution to V_{zz} from the asphericity of the valence-electron charge distribution, which overlaps with the $4f$ shell, the often-used proportionality relation between the EFG and A_2^0 no longer holds anymore. A quantitative discussion of the contributions to A_2^0 from valence electrons will be given elsewhere.[7] In the final section of this paper the implications for hcp Gd and the GdT_2X_2 compounds will be discussed briefly.

II. THEORETICAL METHOD

The electric-field gradient at the nucleus is given by the traceless tensor $V_{ij}=\partial^2 V^*/\partial x_1 \partial x_j$, where V^* is the potential due to electrons in non-s states. In the materials which we will consider in this paper, the main principle axis of the EFG is parallel to the c axis and the asymmetry parameter $\eta=(V_{xx}-V_{yy})/V_{zz}$ is equal to zero. The EFG is then described completely by V_{zz}, which is related to the charge density by

$$V_{zz}=\frac{1}{4\pi\epsilon_0}\int d\mathbf{r}\rho^*(\mathbf{r})\left[\frac{3\cos^2\theta(\mathbf{r})-1}{r^3}\right], \tag{1}$$

where $\rho^*(r)$ is the total charge density minus the contribution from core and valence s states.

A discussion of the various theoretical approaches to V_{zz} in noncubic metals is given in the extensive reviews by Kaufman and Vianden[8] and by Das and Schmidt.[9]

For our calculations of V_{zz} we have used the augmented-spherical-wave method.[10] Exchange and correlation were treated within the local spin-density functional approximation, using the form given by Barth and Hedin,[11] with the parameters given by Janak.[12] The calculations were scalar relativistic, including mass-velocity and Darwin terms. Spin-orbit interaction was neglected. Gd $4f$ states were treated as band states. However, in order to avoid any unphysical population of minority spin $4f$ states, these states were emptied by artificially adding a large positive energy to the corresponding diagonal matrix elements in the Hamiltonian.

Within the ASW method the crystal is subdivided into overlapping spheres within which the potential is spherically symmetric, although the calculated charge density is not spherical. It is natural to separate the calculation of the EFG into a calculation of the valence-electron contribution V_{zz}(val) from the charge density within the central atomic sphere, and the lattice contribution V_{zz}(lat) from the charge density outside this sphere. For the elemental metals, V_{zz}(val) and V_{zz}(lat) are well-defined quantities. In this case, the way in which the crystal is subdivided into spheres belonging to different atoms is fixed because all atomic spheres must have equal radii, and the total volume of the spheres must be equal to the unit-cell volume. However, for compounds there is no unique choice of sphere radii. Therefore, a discussion of V_{zz} in terms of separate quantities V_{zz}(val) and V_{zz}(lat) is only useful if these quantities are rather insensitive to variations of the Gd Wigner-Seitz radius. In Sec. IV, it will be shown that this condition is satisfied for the GdT_2X_2 compounds. The resulting numbers can therefore be used to discuss trends.

Due to the nonuniqueness of the sphere radii, it is not possible to calculate V_{zz}(lat) from a point-charge calculation, using the calculated charges in each of the spheres. A complete calculation of V_{zz}(lat) within the ASW method would involve the calculation of the aspherical charge density within each of the neighboring spheres. Such calculations are much more complex than the calculation of V_{zz}(val), for which only the occupation numbers of orbitals in p and d shells are needed, i.e., the diagonal elements in the density matrix (see below). For V_{zz}(lat) calculations, the interference between orbitals in different shells, which is described by the nondiagonal elements in the density matrix, should also be taken into account. In view of the complexity of such a calculation, we have concentrated on V_{zz}(val), which is the dominant term, as will be shown later, leaving the calculating of V_{zz}(lat) as a future project.

Marathe and Trautwein[13] have shown that V_{zz}(val) can be expressed in the following way as a sum of contributions V_{zz}^p(val) and V_{zz}^d(val) from p and d states:

$$V_{zz}^p(\text{val})=\frac{4}{5}\frac{|e|}{4\pi\epsilon_0}\langle r^{-3}\rangle_p \Delta n_p \tag{2}$$

and

$$V_{zz}^d(\text{val})=\frac{4}{7}\frac{|e|}{4\pi\epsilon_0}\langle r^{-3}\rangle_d \Delta n_d \ . \tag{3}$$

The parameters Δn_p and Δn_d, which give the degree to which the p and d charge densities are prolate or oblate, are defined by

$$\Delta n_p=\tfrac{1}{2}(n_x+n_y)-n_z \tag{4}$$

and

$$\Delta n_d=n_{x^2-y^2}+n_{xy}-\tfrac{1}{2}(n_{xz}+n_{yz})-n_{z^2}\ , \tag{5}$$

where n_x, n_y, and n_z are occupation numbers of the p orbitals and n_{z^2}, n_{xz}, n_{yz}, $n_{x^2-y^2}$, and n_{xy} are occupation numbers of the d orbitals. Furthermore, $\langle r^{-3}\rangle_p$ and $\langle r^{-3}\rangle_d$ are shorthand notations for the radial integrals $\langle R_p|r^{-3}|R_p\rangle$ and $\langle R_d|r^{-3}|R_d\rangle$. R_p and R_d are the radial parts of the valence-electron p- and d-wave functions (e.g., $6p$ and $5d$ for Gd), and the integration extends from $r=0$ to the radius of the Wigner-Seitz sphere. Some technical details concerning the evaluation of V_{zz} will be discussed in the Appendix. For the reader's convenience, we note that the prefactors $\frac{4}{5}|e|/4\pi\epsilon_0$ and $\frac{4}{7}|e|/4\pi\epsilon_0$ in Eqs. (2) and (3) can be replaced by 7.74 and 5.54, respectively, if V_{zz} is expressed in 10^{21} V/m^2, $\langle r^{-3}\rangle$ is expressed in a_0^{-3} (a_0 is Bohr radius), and occupation numbers in electrons/atom.

It is well known that the contributions of the valence and lattice charge density to V_{zz} can be modified by the closed core shells. Often this effect is taken into account

by inserting a radius dependent factor $[1-\gamma(r)]$ into the integrand of Eq. (1), and by subtracting from the charge density $\rho^*(r)$ in Eq. (1) the contribution due to the core states.[9] The factor $[1-\gamma(r)]$ is generally almost equal to unity well inside the core region, whereas it goes steeply to $(1-\gamma_\infty)$ at a radius which is approximately equal to $0.7r_c$, in which r_c is some measure of the core radius.[14] The Sternheimer antishielding factor γ_∞ is defined as $\gamma(r\rightarrow\infty)$. For free rare-earth R^{3+} ions, γ_∞ is approximately -80.[15,16] The antishielding effect is due to "radial excitations" of core states (mainly p states), i.e., a mixing of states with different principle quantum numbers but the same orbital quantum number.[15,17]

As we will show later, the main contribution to V_{zz}(val) comes from the asphericity of the charge density close to the nucleus for which almost no shielding or antishielding is expected. This is confirmed by the results from full potential calculations for hcp metals by Blaha *et al.*,[6] who found only minor core electron contributions to V_{zz}, in all cases less than 10% of the valence contribution. Therefore, we will neglect the (anti)shielding of V_{zz}(val) by core states in our discussions. We finally note that core states could play a more important role in systems with a lower symmetry than the hcp metals, in systems in which they are more extended than in the metals, studied in Ref. 6, and in systems with a large lattice contribution to V_{zz}.

TABLE I. Calculated and experimental values of V_{zz} in hcp metals. The calculational methods (a) and (b) are described in the text. Units: 10^{21} V/m^2. For several metals the sign of V_{zz} has not been measured (indicated with ± sign).

Metal	V_{zz}^{calc} (a)	V_{zz}^{calc} (b)	V_{zz}^{calc} FLAPW[a]	V_{zz}^{expt} (Refs. 6 and 8)
Be	−0.031	−0.015	−0.042	±0.048
Mg	0.046	0.062	+0.048	±0.053
Sc	0.72	0.85	1.0	±0.38
Ti	2.0	2.5	2.1	±1.62
Co	−0.21	−0.22	−0.19	−0.29
Zn	3.4	2.7	3.8	+3.1
Y	2.8	3.17	2.8	
Zr	4.4	5.2	4.3	±3.7
Tc	−1.5	−1.3	−1.5	±0.7
Ru	−1.1	−0.4	−1.2	−0.96
Cd	6.4	5.4	7.6	+7.2
Gd	3.8	5.3		+3.4[b]
Lu	2.6	2.8		+1.08
Hf	10.0	10.4		+9.3
Re	−5.9	−5.4		−4.7
Os	−5.2	−3.4		±3.3
Tl	−0.7	−0.11		

[a]Reference 6.
[b]Reference 20. For the method of calculation of V_{zz} from the measured quadrupole splitting, see text.

III. hcp METALS

We have calculated V_{zz} for all hcp elemental metals, except the heavy rare-earth metals with aspherical $4f$ shells. The reason for performing these calculations is that the calculated values of V_{zz}(val) can be compared directly to the experimental values because V_{zz}(lat) is expected to be small in this case, due to the absence of charge transfer between neighbor atoms. Therefore, the hcp metals are well suited to test our calculational method. The occupation numbers were calculated from the wave functions at 3000 **k** points in the $\frac{1}{24}$ part of the hexagonal Brillouin zone. By performing calculations for such a large number of **k** points, we assured an excellent numerical precision of the calculated occupation numbers. The a and c lattice parameters were taken from Ref. 18.

In Table I, the results of our calculations are compared to the results obtained by Blaha *et al.*, using the full-potential linear augmented-plane-wave (FLAPW) method,[6] and to the experimental data. We have calculated V_{zz} according to two methods. Method (a) has been described in Sec. II. Method (b) is discussed in the Appendix.

Figure 1, which gives V_{zz} [method (a)] as a function of V_{zz}, shows that the overall agreement between theory and experiment is good. In comparing theoretical values with experimental data, it should be noted that in several cases there is some uncertainty about the nuclear quadrupole moment Q which has been used in the evaluation of V_{zz} from the quadrupole splitting. Furthermore, it should be noted that if the sign of V_{zz} has not been experimentally determined, we have chosen the sign of V_{zz} which fitted best to our calculated values. Table I shows that the calculated values of V_{zz} also agree well with the results that were obtained by Blaha *et al.*

A more detailed insight into the origin of the EFG at the nucleus can be obtained from Table II. Qualitatively,

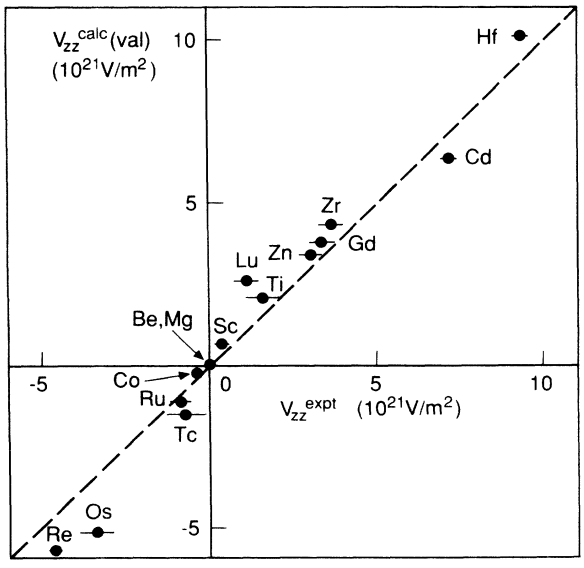

FIG. 1. Calculated valence-electron contribution to V_{zz} in elemental hcp metals vs experimental values of V_{zz}.

TABLE II. Contributions from p and d valence states to V_{zz} in hcp metals. The asphericity parameters Δn_p and Δn_d have been defined in Eqs. (4) and (5). Units: V_{zz} in 10^{21} V/m^2, $\langle r^{-3}\rangle$ in a_0^{-3}.

Metal		Δn_p	Δn_d	$\langle r^{-3}\rangle_p$	$\langle r^{-3}\rangle_d$	V_{zz}^p	V_{zz}^d	V_{zz}^{calc}
Be		−0.008	0.000	0.504	0.148	−0.031	0.000	−0.031
Mg		+0.004	−0.001	1.474	0.060	0.046	0.000	0.046
Sc		+0.023	−0.026	4.72	0.85	0.84	−0.12	0.72
Ti		+0.022	+0.109	6.88	1.38	1.18	0.84	2.0
Co	↑	0.000	−0.005	8.62	5.72	0.00	−0.16	−0.21
	↓	−0.004	+0.008	8.83	5.00	−0.27	+0.22	
Zn		+0.083	−0.004	5.64	9.43	3.64	−0.21	3.4
Y		+0.038	−0.027	10.04	1.10	2.97	−0.16	2.8
Zr		+0.031	−0.087	14.99	1.76	3.61	0.85	4.4
Tc		−0.010	+0.009	22.45	4.20	−1.75	0.21	−1.5
Ru		−0.011	+0.028	22.27	5.02	−1.90	0.81	−1.1
Cd		+0.089	−0.005	9.72	10.29	6.72	−0.29	6.4
Cd[a]		+0.084		11.43		7.47		6.6
Gd	↑	+0.019	+0.027	22.63	2.23	3.32	0.35	3.8
	↓	+0.001	−0.003	24.47	1.76	0.19	−0.03	
Lu		+0.015	−0.025	24.31	2.12	2.84	−0.29	2.6
Hf		+0.028	+0.084	34.33	3.30	8.52	1.51	10.0
Re		−0.017	+0.022	51.18	7.18	−6.77	0.91	−5.9
Os		−0.017	+0.036	51.19	8.70	−6.93	1.73	−5.2
Tl		−0.003	−0.003	20.60	11.09	−0.51	−0.18	−0.7

[a]ASW calculations, Ref. 22. In this paper, Δn_d and $\langle r^{-3}\rangle_d$ were not given. The calculated non-p contribution to V_{zz} was -0.87×10^{21} V/m^2.

the decomposition into p and d contributions to V_{zz}(val) agrees well with the results given by Blaha *et al.* In view of the different sphere radii that were used, a quantitative comparison is not possible.

For gadolinium, the occupation numbers of all orbitals are given in Table III. The calculated total magnetic moment of $7.73\mu_B$/Gd atom is close to the experimental value of $7.63\mu_B$/Gd atom.[19] The calculated value $V_{zz}=3.8\times10^{21}$ V/m^2 is in good agreement with the experimental value of 3.4×10^{21} V/m^2. The latter value has been obtained from the quadrupole splitting (QS) observed by Bauminger *et al.*[20] in ^{155}Gd Mössbauer spectra of single crystals, via the relation $\text{QS}=\frac{1}{2}eQV_{zz}$ and using the quadrupole moment $Q=1.30\times10^{-28}$ m^2 of the ^{155}Gd ground state determined by Tanaka *et al.*[21]

A calculation for hcp Gd in which no artificial shift was applied to $4f$ states (see Sec. II), yielded a total magnetic moment of $7.53\mu_B$/Gd atom, and a (physically unrealistic) $4f^{\downarrow}$ occupancy of 0.13 electrons. Compared to the calculation of V_{zz} presented above, an almost similar value was found: $V_{zz}=3.6\times10^{21}$ V/m^2, the small difference being mainly due to slightly lower values of $\langle r^{-3}\rangle_p$: $19.8a_0^{-3}$ and $21.6a_0^{-3}$ for majority and minority spin electrons, respectively.

TABLE III. Occupation numbers of valence states in hcp Gd obtained from ASW calculations.

nl	Orbitals	Spin up	Spin down
6s	n_s	0.395	0.376
6p	n_x+n_y	0.246	0.128
	n_z	0.104	0.063
5d	$n_{xy}+n_{x^2-y^2}$	0.474	0.216
	$n_{xz}+n_{yz}$	0.404	0.262
	n_{z^2}	0.244	0.088
	Total	1.867	1.133

Table II shows that for most hcp metals the p contribution to V_{zz} is much larger than the d contribution. In several cases, the difference is more than an order of magnitude. In agreement with the explanation given by Blaha *et al.*,[6] we found that the large difference between the $\langle r^{-3}\rangle_p$ and $\langle r^{-3}\rangle_d$ expectation values is due to differences between the distance of the first node in the radial wave functions from the nucleus, and to differences in the shape of the wave functions close to the nucleus. Near the nucleus, the wave functions behave as r^l, which implies that p densities increase more rapidly than d densities. For Gd, the contribution to the $\langle r^{-3}\rangle$ majority spin expectation values, from the charge density outside a sphere with radius r_0, is given in Fig. 2. From this figure and from the occupation numbers given in Table III, we conclude that, for Gd, V_{zz}(val) originates almost completely from the asphericity of the 6p charge density within 0.05 Å from the nucleus.

For Cd our results can also be compared with ASW calculations of the EFG by Schmidt *et al.*[22] (see Table II). Their total value of V^{calc} is close to our total value, but our value of V_{zz}^p is slightly lower than theirs (6.72 and 7.47×10^{21} V/m^2, respectively). The difference is, to a large extent, due to different $\langle r^{-3}\rangle_p$ values. Schmidt *et al.* have used a value of $\langle r^{-3}\rangle$ which was derived directly from the wave functions of the occupied states, and

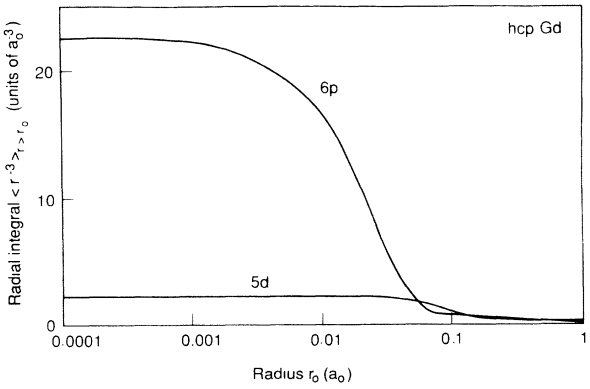

FIG. 2. Radial integrals $\langle r^{-3}\rangle_{r\geq r_0}$ for hcp Gd; a_0 is the Bohr radius (0.5292 Å).

which was averaged over all three p orbitals. This method corresponds to a modification of our method (b), explained in the Appendix, replacing the different $\langle r^{-3}\rangle$ values in Eq. (A1) by an average value. Using this procedure, we find $\langle r^{-3}\rangle_p = 10.31 a_0^{-3}$ and $V_{zz} = 7.10\times 10^{21}$ V/m^2, which is in a better, although not yet perfect, agreement with the value found by Schmidt *et al.* Note that our results, given in Table II, are not based on the charge density, as obtained directly from the occupied states, but on a charge density which follows from a slightly different method [method (a), see Appendix].

IV. COMPOUNDS WITH THE $ThCr_2Si_2$ STRUCTURE

In Sec. III it was shown that for elemental metals with the hcp structure, the asphericity of the valence shells can be calculated quite accurately within the ASW method, resulting in a good overall agreement between calculated and experimental values of V_{zz}. We will now investigate the accuracy of our method for a large series of intermetallic compounds of the type GdT_2Si_2 ($T=3d$, $4d$, and $5d$ transition metals) and $GdNi_2X_2$ (X=Si, Ge, and Sn). The body-centered tetragonal unit cell of their $ThCr_2Si_2$ structure is shown in Fig. 3. Rare-earth atoms occupy sites at the corners and at the center of the cell. Each rare-earth atom has eight T neighbors and eight X neighbors.

Hyperfine parameters of the GdT_2Si_2 compounds, which were obtained by ^{155}Gd Mössbauer spectroscopy, were reported recently by Dirken *et al.*[4] As shown in Fig. 4, V_{zz} was found to increase with increasing filling of the d band of the T atoms. We have performed additional measurements for $GdNi_2Ge_2$ and $GdNi_2Sn_2$. The experimental details are similar to those described in Ref. 4. For both compounds, the fitting procedure was performed with the effective hyperfine field perpendicular to the c axis. Values for the various hyperfine parameters are given in Table IV. The ^{155}Gd Mössbauer spectra and their fits are shown in Fig. 5, in which, for comparison, the spectrum for $GdNi_2Si_2$ is also given. In the present paper, the discussion is concentrated on V_{zz}. Trends in

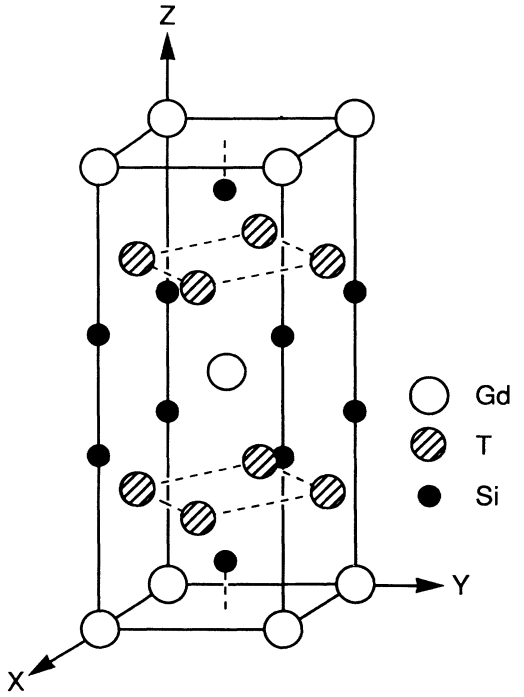

FIG. 3. Unit cell of the $ThCr_2Si_2$ structure.

the Gd hyperfine fields and isomer shifts are still being studied, and will be discussed elsewhere.

Dirken *et al.*[4] have mentioned that the observed variations of V_{zz} across the three series of GdT_2Si_2 ($T=3d$, $4d$, or $5d$) cannot be understood from the variation of V_{zz}(lat), which is expected from the elec-

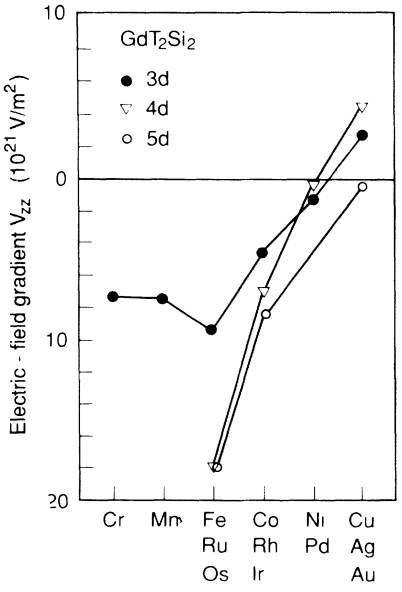

FIG. 4. Experimental values of V_{zz} at Gd nuclei across the three series of compounds of the type GdT_2Si_2 ($T=3d$, $4d$, or $5d$).

TABLE IV. Hyperfine parameters derived from fits of the ^{155}Gd Mössbauer spectra of $GdNi_2Si_2$, $GdNi_2Ge_2$, and $GdNi_2Sn_2$ measured at 4.2 K.

Compound	V_{zz} (10^{21} V/m^{-2})	B_{hf} (T)	Isomer shift (mm/s)
$GdNi_2Si_2$	−1.2(1)	26.9(2)	0.57(1)
$GdNi_2Ge_2$	−1.6(2)	32.2(2)	0.58(1)
$GdNi_2Sn_2$	−6.2(2)	17 (2)	0.52(2)

tronegativity of the T atoms. In order to explain in this way the increase of V_{zz} for T=Fe to T=Ni (and similarly from Ru to Pd and from Os to Pt), it would be necessary to assume a *large increase* (towards more positive values) for the charge of the T atoms. However, in reality, large changes of the effective charge of the T atoms are unphysical, since the electronegativity differences between the late transition metals are quite small. Moreover, at the end of each transition-metal series (e.g., from Fe to Ni), the electronegativity increases, which is expected to result in a *decrease* of the charge of the T atoms with respect to Gd and Si.

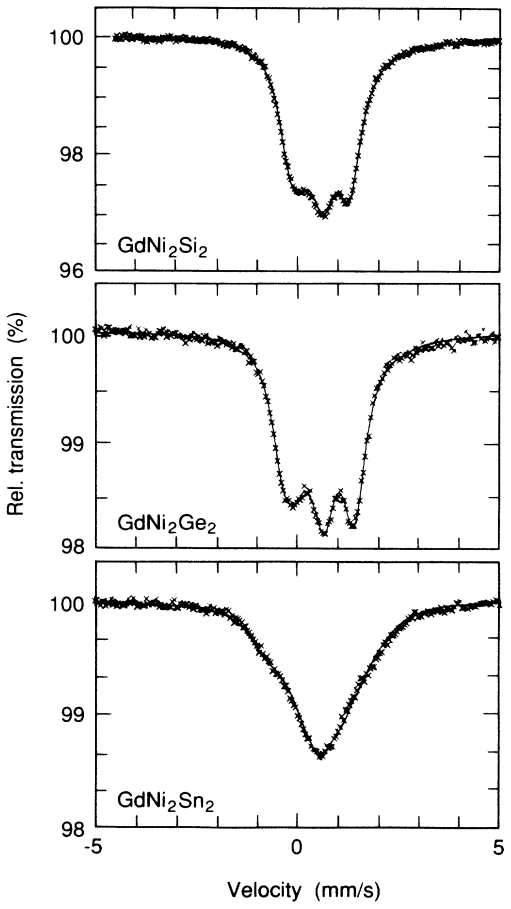

FIG. 5. ^{155}Gd Mössbauer spectra of $GdNi_2X_2$ compounds (X=Si, Ge, and Sn). The lines through the data points represent fits to the spectra.

In order to investigate valence-electron contributions to V_{zz}, we have also performed ASW band-structure calculations. The crystal-structure data for GdT_2Si_2 compounds were taken from Ref. 23. For $GdNi_2Ge_2$ and $GdNi_2Sn_2$ we used a=4.066 and 4.370 Å, respectively, and c/a=2.41 and 2.22, respectively. These values were obtained by x-ray diffraction on powder specimens. The z parameter, which specifies the position of the Si (or Ge, Sn) atoms at (0,0,z) and equivalent sites, has not been measured for most compounds. In all cases we took z=0.38. The experimental values of z are within the range 0.37–0.39. From calculations of V_{zz}, using z=0.37 or 0.39, we found deviations of, at most, 6% from the EFG, calculated for z=0.38. In order to obtain an optimal representation of the real charge density in our ASW calculations, we have used values of $r_{WS}\simeq 1.86$ Å for Gd, $r_{WS}\simeq 1.50$ for Si, and Wigner-Seitz radii for the T atoms that were approximately equal to the values in the elemental metals. The radius for Gd was taken to be smaller than the radius in the elemental metal (1.99 Å) in order to take into account its high compressibility and its tendency to lose some of its valence electrons, being a relatively electropositive atom. This choice resulted in approximately zero ($\pm 0.2e$) total charge in the Gd spheres. For the $ThCr_2Si_2$ structure, the sphere radii that were used led to a good filling of space, with no excessive overlap between spheres nor large empty regions. Occupation numbers were obtained from calculations for 154 **k** points in the irreducible part of the Brillouin zone.

In Fig. 6, the calculated values of V_{zz}(val) are plotted as a function of the experimental values. It is clear from this figure that the observed trend in V_{zz} can be well explained from the variation of V_{zz}(val). This means that V_{zz} is apparently determined to a large extent by the as-

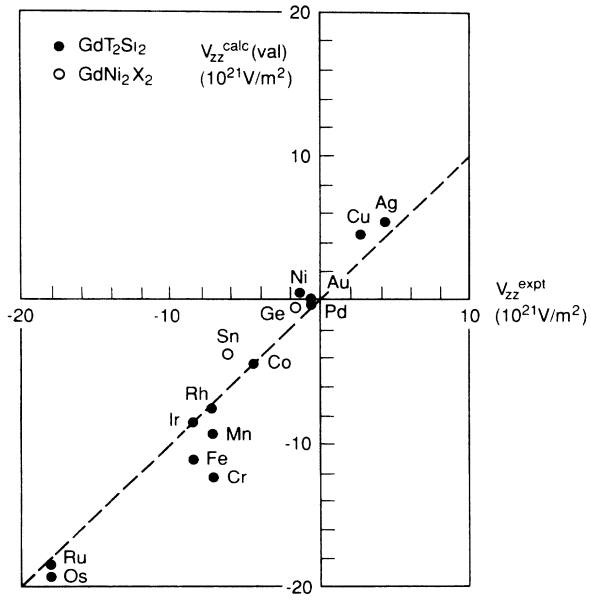

FIG. 6. Calculated valence-electron contribution to V_{zz} in GdT_2Si_2 (T=3d, 4d, or 5d) and in $GdNi_2X_2$ (X=Si, Ge, Sn) compounds vs experimental values of V_{zz}.

phericity of the charge density within about 1.86 Å of the nucleus. The largest differences are found for T atoms in the $3d$ series. In particular, for $GdCr_2Si_2$, there is a relatively large difference between V_{zz}^{calc}(val) and V_{zz}^{expt}. We will come back to this point later. Calculations for $GdRu_2Si_2$ and $GdAg_2Si_2$, in which r_{WS}(Gd) was decreased by 0. 11 to 1.74 and 1.78 Å, respectively, revealed a change of V_{zz}(val) of only $+1.3$ and $+0.3\times10^{21}$ V/m^2, respectively. V_{zz} was also found to be rather insensitive to variations in the ratio of the radii of the T and Si spheres. Due to the weak dependence of V_{zz}(val) on the sphere radii, it can be considered as a useful quantity.

The decomposition of V_{zz}(val) into contributions from $6p$ and $5d$ shells in Table V shows that the $6p$ contribution dominates V_{zz}(val) because $\langle r^{-3}\rangle_{6p}$ is much larger than $\langle r^{-3}\rangle_{5d}$, whereas the asphericities of p and d shells are of the same order of magnitude. The same situation was found in Sec. III for hcp Gd. For most compounds, $\langle r^{-3}\rangle_{6p\uparrow}$, $\langle r^{-3}\rangle_{6p\downarrow}$, $\langle r^{-3}\rangle_{5d\uparrow}$, and $\langle r^{-3}\rangle_{5d\downarrow}$ were approximately equal to 35, 40, 2.0, and $1.6a_0^{-3}$, respectively. These values of $\langle r^{-3}\rangle$ cannot be compared directly with those for the Gd metal because different Wigner-Seitz radii of the Gd spheres were used. In Fig. 7, the variation across the three transition-metal series of the asphericities Δn_p and Δn_d (as defined in Sec. II) are given for GdT_2Si_2 compounds. It can be seen that the reversal of the sign of the contribution to V_{zz} from p and d shells takes place at different positions within the transition-metal series. This different behavior of Δn_p and Δn_d will be important in the discussion of the relationship between V_{zz} and A_2^0 (see Sec. VI).

In Fig. 7 the contributions from majority and minority spin electrons were averaged. For p electrons both contributions were found to be nearly identical, except in the case of $GdMn_2Si_2$, where we found a Mn spin magnetic moment of $1.9\mu_B$ coupled antiparallel to the Gd moments. The two contributions to Δn_p are given separately in Fig. 7. For $5d$ electrons the contributions to V_{zz} from majority and minority spin electrons exhibited much larger differences than for $6p$ electrons. Nevertheless, the trends in Δn_d are the same for both spin directions, which led us to present only the average contribu-

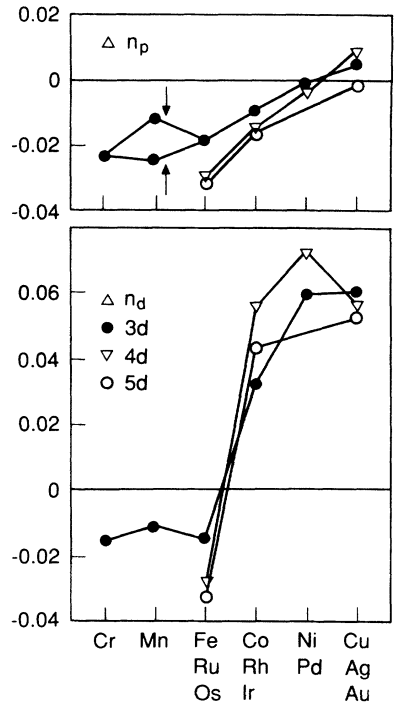

FIG. 7. Variations of asphericities Δn_p and Δn_d of $6p$ and $5d$ shells of Gd in GdT_2Si_2 compounds ($T=3d$, $4d$, and $5d$ transition-metal atoms).

TABLE V. Contributions from $6p$ and $5d$ valence states to V_{zz} in GdT_2Si_2 and $GdNi_2X_2$ compounds. Units V_{zz}: 10^{21} V/m^2.

	$V_{zz}^{p(\uparrow)}$	$V_{zz}^{p(\downarrow)}$	$V_{zz}^{d(\uparrow)}$	$V_{zz}^{d(\downarrow)}$	$V_{zz}^{(val)}$	V_{zz}^{expt}
$GdCr_2Si_2$	−5.8	−6.3	−0.1	−0.1	−12.3	−7.1
$GdMn_2Si_2$	−6.0	−3.0	−0.2	−0.0	−9.2	−7.2
$GdFe_2Si_2$	−4.7	−6.2	−0.1	−0.2	−11.2	−9.3
$GdCo_2Si_2$	−2.5	−2.5	+0.5	+0.2	−4.3	−5.3
$GdNi_2Si_2$	−0.6	−0.3	+0.7	+0.5	+0.3	−1.2
$GdCu_2Si_2$	+1.4	+2.2	+0.6	+0.6	+4.8	+2.8
$GdRu_2Si_2$	−8.3	−9.3	−0.3	−0.3	−18.2	−18.4
$GdRh_2Si_2$	−4.3	−4.5	+1.0	+0.2	−7.6	−7.6
$GdPd_2Si_2$	−1.4	−0.3	+0.9	+0.6	−0.2	−0.6
$GdAg_2Si_2$	+1.7	+2.4	+0.6	+0.6	+5.3	+4.3
$GdOs_2Si_2$	−8.9	−9.7	−0.4	−0.3	−19.3	−18.5
$GdIr_2Si_2$	−4.6	−4.9	+0.8	+0.2	−8.5	−8.4
$GdAu_2Si_2$	−0.7	−0.4	+0.6	+0.5	0.0	−0.5
$GdNi_2Si_2$	−0.6	−0.3	+0.7	+0.5	+0.3	−1.2
$GdNi_2Ge_2$	−1.0	−0.7	+0.8	+0.5	−0.4	−1.6
$GdNi_2Sn_2$	−2.5	−1.7	+0.3	+0.2	−3.7	−6.0

tion in Fig. 7.

We should emphasize that, for all calculations, a ferromagnetic coupling between the moments was assumed, whereas in reality most compounds show an antiferromagnetic spin structure. In general, this is not expected to result in large errors because for most compounds the induced magnetizations on the T and X atoms were less than $0.1\mu_B$, indicating a very weak coupling between the moments. However, for cases like $GdCr_2Si_2$ and $GdMn_2Si_2$, it might be very important to perform the calculations within the proper magnetic structure. As remarked already, for $GdCr_2Si_2$ the difference between V_{zz}(val) and V_{zz} is rather large. We found a stable solution with $m(\mathrm{Cr})=-0.06\mu_B$ (moment antiparallel to Gd), but, by starting the iterative calculation with a different potential, we also found a metastable solution with $m(\mathrm{Cr})=-0.82\mu_B$. The values of V_{zz}(val) were almost identical. However, the existence of this metastable solution, and the high-Cr $3d$ partial density of states at the Fermi level for the stable solution (1.5 states eV^{-1} $\mathrm{atom}^{-1}\,\mathrm{spin}^{-1}$), suggest that other, magnetically more complex solutions could be more stable, resulting in a different value for V_{zz}. It is also possible that the actual value of V_{zz} is larger than the value given in Table IV, if the Gd moments are not directed exactly parallel to the c axis, as was assumed in the analysis of the Mössbauer spectrum for $GdCr_2Si_2$.

V. ORIGIN OF THE ASPHERICITY OF RARE-EARTH VALENCE SHELLS

In Sec. IV it was shown by band-structure calculations that the increase in V_{zz} across each of the transtion-metal series GdT_2Si_2, and the decrease of V_{zz} in the series $GdNi_2X_2$ (X=Si, Ge, Sn), can be explained by a change of the asphericity of the rare-earth valence shells. This trend can be explained in two, complementary, ways.

First, we will analyze the hybridization between Gd p and d states on the one hand, and T metal d states on the other hand. The centers of the Gd $6p$ and $5d$ bands are situated above the Fermi level, whereas the center of the d band of the T atom is situated below the Fermi level and lowers when going towards the end of each transition-metal series. This implies that the hybridization between Gd valence states and T atom d states, which leads to the formation of bonding orbitals with large charge densities between the Gd and T atoms, becomes weaker towards the end of each transition-metal series. The Gd orbitals that take part in this hybridization are primary those whose charge cloud is directed towards the T atoms, i.e., p_z and d_{xz}/d_{xz} orbitals. Indeed, for compounds with $4d$ T atoms, n_z decreases linearly from 0.133 for T=Ru to 0.098 for T=Ag, whereas n_x and n_y remain constant at 0.103. The situation is slightly more complicated for d orbitals. As expected, n_{xz} and n_{yz} decrease from T=Ru to Pd. However, n_{xy} increases strongly from T=Ru to Rh (from 0.135 to 0.208). From an inspection of the T $4d$ and the Gd $5d$ partial density of states, we found that the Gd $5d_{xy}$ states are hybridized with $4d$ states of the T atoms which cross the Fermi level between T=Ru and Rh. This results in a large jump of Δn_d (see Fig. 7). For T=Cr and Mn, V_{zz} does not decrease further with decreasing atomic number, because, in this case, the part of the transition-metal $3d$ band in which the Gd $6p-t$ $3d$ bonding states are found is not yet completely situated below the Fermi level.

A second approach to explain the variation of the asphericity of the valence shells of Gd atoms is based on a consideration of the charge density at the edge of the atomic cell. We will present a simple treatment of the electronic structure, based on Miedema's "macroscopic-atom" model for cohesion in metals.[24] Within this model, one of the contributions to the heat of formation of an alloy is the energy that is required to eliminate the discontinuity of the charge density at the boundary of the atomic cell. Processes in the central atom which lead to a change in the charge density at the cell boundary are volume changes, charge redistribution between s, p, and d states, and between orbitals with the same l quantum number. Only the latter process leads to a change of the asphericity of the charge density.

Within the "macroscopic-atom model," the average charge density n_{WS} at the edge of the atomic cells has been given as model parameters for all elements.[24] The values of n_{WS} are strongly correlated with the actual charge densities at the edge of the atomic spheres in the elemental metals, which follow from first-principles band-structure calculations.[25] In our discussion of the asphericity of the rare-earth valence-electron charge distribution, we will assume that the charge density at the edge of the rare-earth atomic cell will adjust itself to match the charge density at the edge of the Si cells and the transition-metal cells. In view of the crystal structure, the contribution to which V_{zz} arises from the aspherical valence shells is therefore expected to be related to $\Delta n_{\mathrm{WS}}=n_{\mathrm{WS}}(T)-n_{\mathrm{WS}}(\mathrm{Si})$. A large value of $n_{\mathrm{WS}}(T)$ is expected to lead to a large negative value of V_{zz}. For the compounds in the series GdT_2Si_2, V_{zz} has been plotted as a function of Δn_{WS} in Fig. 8, which confirms the expected correlation. For Ni and Pd the agreement is not satisfactory. The reason is that in $GdNi_2Si_2$ and $GdPd_2Si_2$ the localized part of the transition-metal d shell is completely occupied. The Miedema values of n_{WS} for Ni and Pd are more suitable for alloys in which the d bands are not entirely occupied. With increasing d-band filling, the Ni and Pd ions become electronically more similar to Cu and Ag, respectively, which have low n_{WS} values. In the figure, we have indicated the direction of the corresponding correction of Δn_{WS} by arrows. In $GdMn_2Si_2$, the Mn atoms have a moment of the order of $2\mu_B$. The electronic structure at the Mn site is expected to resemble the electronic structure of Fe (spin-up electrons) and Cr (spin-down electrons). Therefore, we have used

$$n_{\mathrm{WS}}(\mathrm{Mn})=\tfrac{1}{2}[n_{\mathrm{WS}}(\mathrm{Fe})+n_{\mathrm{WS}}(\mathrm{Cr})]\ .$$

From the relation between Δn_{WS} and V_{zz} it can be understood why V_{zz} for $GdCr_2Si_2$ and $GdMn_2Si_2$ is less negative than for $GdFe_2Si_2$. Furthermore, the decrease of V_{zz} in the series $GdNi_2X_2$ (X=Si, Ge, Sn) can also be explained qualitatively, because for these compounds Δn_{WS}

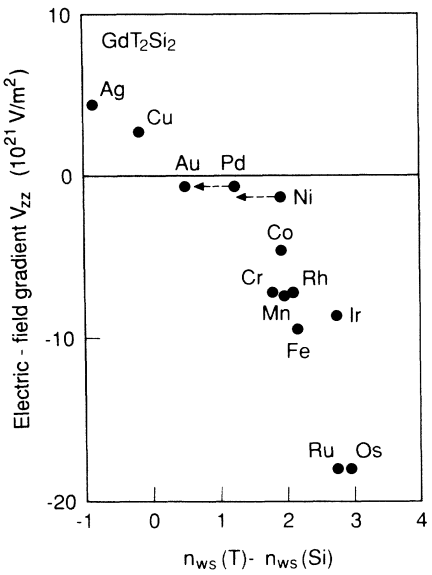

FIG. 8. Dependence of experimental values of V_{zz} of GdT_2Si_2 compounds on the difference of the electron density n_{WS} at the edge of the atomic cell of T and Si atoms, within Miedema's model (Ref. 24).

is 1.98, 2.79, and 3.46, respectively.

The model for $V_{zz}(\text{val})$ that was presented above implies that in cases for which the T and X sites are occupied with identical atoms, $V_{zz}(\text{val})$ is not expected to depend on the type of these atoms. In order to test this prediction, we have performed calculations for the hypothetical $GdRu_4$ and $GdSi_4$ compounds, using the unit-cell parameters and Wigner-Seitz sphere radii that were used for $GdRu_2Si_2$. Si and Ru were selected because their atomic volumes are nearly equal, whereas their n_{WS} values are strongly different. For both compounds we found $V_{zz}(\text{val}) = -4.7\times10^{21}$ V/m^2, whereas the contributions from the p and d shells to V_{zz} were also almost identical. This supports the model presented above.

We conclude that trends in the asphericity of rare-earth valence shells can be well understood from a consideration of the local environment, i.e., from a consideration of the position and type of nearest neighbors only. An important parameter which characterizes the neighbor atoms is their "electron density at the edge of the atomic sphere," as given by the Miedema parameter n_{WS}. The asphericity of the rare-earth valence shells is determined by this parameter through the demand of continuity in the charge density. Modifications to this simple picture are found to be necessary if, due to crystallographic peculiarities, the bands which contain the states which take part in the bonding process show an appreciable fine structure. The consideration of such details is necessary to explain the variation of the $5d$ contribution to V_{zz} in GdT_2Si_2 compounds.

VI. CONCLUDING REMARKS

It was shown that the EFG in hcp metals and at Gd nuclei in GdT_2X_2 compounds can be well understood from the asphericity of the valence shells. The contribution to V_{zz} from the region outside the central Wigner-Seitz sphere was not calculated. For hcp metals, this contribution is expected to be small because charge-transfer effects are absent. This is supported by the good agreement between $V_{zz}^{\text{calc}}(\text{val})$ and V_{zz}^{expt}. In the case of GdT_2X_2 compounds, from the comparison between $V_{zz}^{\text{calc}}(\text{val})$ and V_{zz}^{expt}, one can derive that an upper limit for $V_{zz}(\text{lat})$ is approximately 2.10^{21} V/m^2. Except possibly for $GdNi_2Si_2$, $GdNi_2Ge_2$, $GdPd_2Si_2$, and $GdAu_2Si_2$, $|V_{zz}(\text{val})|$ is always larger than $|V_{zz}(\text{lat})|$.

The EFG at Gd nuclei is dominated by the asphericity of the p shell. The asphericity of this shell, and to some degree also of the d shell, was described successfully within a simple picture of the local electronic structure, in which the main parameter characterizing the neighbor atoms was the "electron density at the edge of the atomic sphere," as given, e.g., by the Miedema parameter n_{WS}. If the position of the neighbors with the highest value of n_{WS} is within or close to the plane perpendicular to the c axis, containing the Gd atoms, V_{zz} is expected to be positive, whereas V_{zz} is expected to be negative if these neighbors are situated on or close to the line through the Gd atom which is parallel to the c axis. This rule is very helpful in obtaining an understanding of variations of V_{zz} in Gd-T-B ternary compounds (T=Fe, Co), as we will show in a subsequent paper.[7] In this paper we will also discuss why, in several series of compounds, the point-charge model gives such a good description of the variations of V_{zz}.

In Fig. 2 we showed that the contribution to $V_{zz}(\text{val})$ from p and d shells is mainly due to the asphericity of the part of these shells which is situated within 0.05 Å from the nucleus. In contrast, the asphericity of the valence-electron charge density within this radius contributes little to the crystal-field parameters A_n^m because the $4f$ shell is situated well outside this radius. Figure 2 suggests that the sensitivity of A_2^0 in hcp Gd to a certain degree of asphericity Δn_p or Δn_d of p and d shells is of the same order of magnitude because, in the region of interest, for $0.1 \le r_0 \le 2a_0$, $\langle r^{-3}\rangle_{r>r_0}$ is quite similar for the $6p$ and $5d$ states. This will be shown in a subsequent paper in which the valence-electron contribution to A_2^0 will be derived from band-structure calculations.[7]

The main implication of our results is that the relation

$$A_2^0 = -\frac{1}{4}\frac{(1-\sigma_2)}{(1-\gamma_\infty)}V_{zz}\ , \tag{6}$$

which is often used within the framework of the point-charge model,[1-3] lacks a true physical basis. The factor $(1-\sigma_2)$ in this relation has been interpreted as a shielding factor, representing the shielding of the point charges by the valence electrons of the central atom. Usually, $(1-\sigma_2)$ is taken to be approximately equal to 0.5. Our analysis of the EFG in GdT_2Si_2 compounds had led to the conclusion that, for most of these compounds, V_{zz} is dominated by $V_{zz}(\text{val})$, and that the valence-electron contributions to V_{zz} and A_2^0 are determined in quite different ways by the asphericities of the $6p$ and $5d$ shells. Due to

the latter effect, it is even possible that the sign of A_2^0 that is predicted from the experimental sign of V_{zz}, using Eq. (6), is wrong. This situation can occur if the signs of Δn_p and Δ_d are different. Table III shows that, for hcp Gd, this is not the case. However, Fig. 7 shows that such a situation might arise for various GdT_2Si_2 compounds. For these compounds, further calculations are necessary to obtain the sign of the valence-electron contribution to A_2^0.

ACKNOWLEDGMENTS

The authors have benefitted from discussions about the origin of the asphericity of rare-earth valence shells with A. R. Miedema.

APPENDIX

In this appendix, a technical detail concerning the evaluation of $\langle r^{-3}\rangle$ expectation values within the ASW method is discussed. In Sec. III, we performed direct calculations of $\langle r^{-3}\rangle$ radial expectation values and of $V_{zz}(\mathrm{val})$ for hcp metals based on the eigenfunctions of the occupied states. This method was called (*b*). Within this method, the differences in the $\langle r^{-3}\rangle_{lm}$ values of subshells with the same l quantum number, but with different azimuthal quantum numbers m, are taken into account. Note that these differences were neglected in the derivation of Eqs. (2) and (3) from Eq. (1). In method (*b*) we have used the modified expression

$$V_{zz}^{p}(\mathrm{val})=\frac{4}{5}\frac{|e|}{4\pi\epsilon_0}\left(\tfrac{1}{2}[\langle r^{-3}\rangle_{p_x}n_x+\langle r^{-3}\rangle_{p_y}n_y]-\langle r^{-3}\rangle_{p_z}n_z\right) \quad \text{(A1)}$$

instead of Eq. (2), and a similar modification of Eq. (3) was used for $V_{zz}(\mathrm{val})$.

Within the ASW method, a wave function of a state with energy $E(\mathbf{k})$ is the sum of l-dependent wave functions whose radial parts are each a linear combination of the augmentations within the Wigner-Seitz sphere of spherical Bessel and Hankel functions. The l-dependent radial wave functions each correspond to an energy $E_l(\mathbf{k})$. In general, these energies $E_l(\mathbf{k})$ are not equal to $E(\mathbf{k})$. If the eigenstate that is considered is dominated by a certain value l', then $E_{l'}(\mathbf{k})$ will be close to $E(\mathbf{k})$, but the energies $E_l(\mathbf{k})$ for the other l values can differ considerably. Therefore, the electron density which follows directly from the wave functions of the occupied eigenstates is a less reliable aspect of the calculations than the eigenvalues. The ASW method uses a different procedure for the calculation of the charge density within a certain atomic sphere. It is based on radial wave functions which are evaluated at the actual energy E of the occupied states, using the partial density of states (in practice, this method is further simplified, see Ref. 10). On the one hand, this method is expected to yield an improvement of the radial charge density, but on the other hand, differences in the radial charge density for states with different azimuthal quantum numbers are neglected. The calculational method, in which $\langle r^{-3}\rangle_l$ values are obtained from this spherical charge density, has been called method (*a*) in Sec. III.

Table I shows that the results which have been obtained by method (*a*) are generally in better agreement with the FLAPW results, obtained by Blaha *et al.*, than the results that were calculated by method (*b*). Therefore, we have decided to perform calculations of GdT_2Si_2 compounds using method (*a*).

[1]M. Bogé, G. Czjzek, D. Givord, C. Jeandry, H. S. Li, and J. L. Oddou, J. Phys. F **16**, L67 (1986).
[2]H. H. A. Smit, R. C. Thiel, and K. H. J. Buschow, J. Phys. F **18**, 295 (1988).
[3]M. W. Dirken, R. C. Thiel, and K. H. J. Buschow, J. Less Common Met. **146**, L15 (1989).
[4]M. W. Dirken, R. C. Thiel, and K. H. J. Buschow, J. Less Common Met. **147**, 97 (1989).
[5]M. W. Dirken, R. C. Thiel, L. J. de Jongh, T. H. Jacobs, and K. H. J. Buschow, J. Less Common Met. (to be published).
[6]P. Blaha, K. Schwarz, and P. H. Dederichs, Phys. Rev. B **38**, 9368 (1988).
[7]R. Coehoorn, Phys. Rev. B **41**, 11 790 (1990).
[8]E. N. Kaufman and R. J. Vianden, Rev. Mod. Phys. **51**, 161 (1979).
[9]T. P. Das and P. C. Schmidt, Z. Naturforsch. **41A**, 47 (1986).
[10]A. R. Williams, J. Kübler, and C. D. Gelatt, Jr., Phys. Rev. B **19**, 6094 (1979).
[11]U. von Barth and L. Hedin, J. Phys. C **5**, 1629 (1972).
[12]J. F. Janak, Solid State Commun. **25**, 53 (1978).
[13]V. R. Marathe and A. Trautwein, in *Advances in Mössbauer Spectroscopy*, edited by B. V. Thosar, P. K. Iyengar, J. K. Srivastava, and S. C. Bhargava (Elsevier, Amsterdam, 1983), p. 423.
[14]K. W. Lodge, J. Phys. F **6**, 1989 (1976).
[15]R. M. Sternheimer, Phys. Rev. **146**, 140 (1966).
[16]K. D. Sen, P. C. Schmidt, and A. Weiss, Z. Naturforsch. **419**, 37 (1986).
[17]A. J. Freeman and R. E. Watson, in *Magnetism*, edited by G. T. Rado and H. Suhl (Academic, New York, 1965), Vol. IIA, p. 177.
[18]P. Villars and L. D. Calvert, *Pearson's Handbook of Crystallographic Data for Intermetallic Phases* (American Soc. Metals, Metals Park, OH, 1985).
[19]S. Legvold, in *Ferromagnetic Materials*, edited by E. P. Wohlfahrt (North-Holland, Amsterdam, 1980), Vol. 1, p. 216.
[20]E. R. Bauminger, A. Diamant, I. Felner, I. Nowik, and S. Ofer, Phys. Rev. Lett. **34**, 962 (1975).
[21]Y. Tanaka, D. B. Laubacher, R. M. Steffen, E. B. Shera, H. D. Wohlfahrt, and M. V. Hiehn, Phys. Lett. **108B**, 8 (1982).
[22]P. C. Schmidt, A. Weiss, S. Cabus, and J. Hübler, Z. Naturforsch. **42a**, 1321 (1987).
[23]K. H. J. Buschow and D. B. de Mooij, Philips J. Res. **41**, 55 (1986).
[24]F. R. de Boer, R. Boom, W. C. M. Mattens, A. R. Miedema, and A. K. Niessen, *Cohesion in Metals, Transition Metal Al-*

loys (North-Holland, Amsterdam, 1988).

[25]D. G. Pettifor, in *Solid State Physics,* edited by H. Ehrenreich and D. Turnbull (Academic, Orlando, 1987), Vol. 40, p. 43. In Fig. 25 calculated electron densities at the edge of the Wigner-Seitz sphere are shown that were obtained from unpublished results from A. R. Williams, C. D. Gelatt, and V. L. Moruzzi (1980).